

Atomic potential energy uncertainty in machine-learning interatomic potentials and thermal transport in solids with atomic diffusion

Yifan Zhu,^{1,2,3,*} Erting Dong,^{3,4,*} Hongliang Yang,^{1,2,3,*} Lili Xi,^{5,6} Jiong Yang^{5,6,†} and Wenqing Zhang^{3,1,7,‡}

¹State Key Laboratory of High Performance Ceramics and Superfine Microstructure, Shanghai Institute of Ceramics, Chinese Academy of Sciences, Shanghai 200050, China

²University of Chinese Academy of Sciences, Beijing 100049, China

³Department of Materials Science and Engineering, Southern University of Science and Technology, Shenzhen, Guangdong 518055, China

⁴College of Materials Science and Engineering, Henan Institute of Technology, Xinxiang, Henan 453000, China

⁵Materials Genome Institute, Shanghai University, Shanghai 200444, China

⁶Zhejiang Laboratory, Hangzhou, Zhejiang 311100, China

⁷Shenzhen Municipal Key-Lab for Advanced Quantum Materials and Devices, and Guangdong Provincial Key Lab for Computational Science and Materials Design, Southern University of Science and Technology, Shenzhen, Guangdong 518055, China



(Received 9 May 2023; accepted 11 July 2023; published 24 July 2023)

Thermal transport simulations have attracted wide attention in recent years, and one standard approach is to use the Green-Kubo method based on machine-learning interatomic potentials and equilibrium molecular dynamics (GK-MLIP-EMD). In this work, we focus on the lattice thermal conductivities κ_{LS} for solids with atomic diffusion by taking β -Cu_{2-x}Se ($0 \leq x \leq 0.05$) as an example. Surprisingly, the GK-MLIP-EMD approach fails in the evaluation of κ_{LS} for β -Cu_{1.95}Se, whereas the direct method based on nonequilibrium molecular dynamics reliably predicts these values instead. The failure of GK-MLIP-EMD for β -Cu_{1.95}Se could be attributed to the ambiguous projection of the local atomic potential energy U_i in MLIPs, exacerbated by the Cu diffusion at elevated temperatures. The Cu diffusion in β -Cu_{1.95}Se greatly increases the ratio of the convective term and the uncertainty of the conductive term. These influences are considered negligible in crystalline solids. Our findings imply that the ambiguous definition of U_i in MLIPs breaks down the applicability of the GK-MLIP-EMD approach to κ_L prediction for solids with severe atomic diffusion.

DOI: [10.1103/PhysRevB.108.014108](https://doi.org/10.1103/PhysRevB.108.014108)

I. INTRODUCTION

Controlling thermal transport is a fundamental issue in material applications. Electron devices require high-thermal-conductivity materials, while low-thermal-conductivity materials are favorable for thermoelectric applications [1]. Accurately predicting the lattice thermal conductivities κ_{LS} provides constructive guidance for optimizing the thermal transport properties of materials [2]. The Boltzmann transport equation (BTE) based on the perturbation theory framework clearly describes phonon transport and has been successfully implemented in simulating the thermal transport of crystalline materials [3,4]. Even for crystalline systems with strong anharmonicity, precise κ_{LS} can also be obtained by the BTE method by considering higher-order phonon scattering [5,6].

There is a special class of solid materials that does not have fixed equilibrium atomic positions for fractions of atoms, such as part-crystalline part-liquid (PCPL) β -Cu₂Se [7,8]. Cu_{2-x}Se has attracted abundant research attention as a promising thermoelectric material. This compound has a structural phase transition at approximately 400 K [9,10].

The structure of low-temperature phase α -Cu₂Se remains controversial, and Qiu *et al.* [11] have reported the coexistence of various structures according to density functional theory (DFT) calculations. High-temperature phase β -Cu₂Se is a superionic conductor, and Cu ions are kinetically disordered throughout the crystal lattice [9]. The unique structure leads to abnormal thermal transport and extremely low κ_L .

However, theoretical research on the thermal transport in β -Cu_{2-x}Se is challenging due to the superionic nature and the common existence of Cu atomic vacancies [9]. The BTE method based on small displacements completely breaks down for β -Cu_{2-x}Se. Molecular dynamics (MD) simulation [12] provides a feasible way to study the thermal transport properties of β -Cu_{2-x}Se, as well as other solid materials. The MD methods can be divided into the Green-Kubo [13,14] (including convective and conductive terms) method based on equilibrium molecular dynamics (EMD) and the direct method [15–17] based on nonequilibrium molecular dynamics (NEMD). Furthermore, all thermal transport simulations based on MD demand an accurate description of the atomic interactions, which usually entails DFT-based and/or empirical potentials. However, the precise DFT-based interatomic potentials are computationally prohibitive for large cells with atomic numbers larger than 1000, while fast empirical potentials with simplified interatomic interactions are not suitable

*These authors contributed equally to this work.

†Corresponding author: jiongy@t.shu.edu.cn

‡Corresponding author: zhangwq@sustech.edu.cn

for thermal transport simulations of complex systems such as β -Cu_{2-x}Se.

Machine-learning interatomic potentials (MLIPs) combine the advantages of DFT-based and empirical potentials in thermal transport simulations of complex materials. Various MLIP forms have emerged in recent years, such as the high-dimensional potential energy surface [18], Gaussian approximation potential [19], deep potential molecular dynamics [20], and moment tensor potential (MTP) [21]. Meanwhile, active learning methods, such as deep potential generator [22] and dual adaptive sampling (DAS) [23], have been developed to generate effective training data sets and further construct accurate MLIP models. MLIPs have been utilized in the fields of phase diagrams [24], catalysis [25], thermal transport [26,27], and so on. The total potential energy and forces predicted by MLIPs are comparable to DFT calculation results, and MLIPs are suitable for thermal transport in complex materials.

Although the Green-Kubo approach based on machine-learning interatomic potentials and equilibrium molecular dynamics (GK-MLIP-EMD) is one of the standard solutions for simulating the thermal transport of complex solid materials, thermal transport studies of materials with superionic conductor characteristics have not been discussed. Reportedly, the Green-Kubo method is not suitable for multicomponent fluids [28,29], indicating a potential risk when applying it to the thermal transport of superionic conductors. In this work, we select PCPL β -Cu_{2-x}Se and full-crystalline compounds Mg₃Sb₂ (see more details in our previous work [23]), and Mg₂Sn as typical examples to discuss the applicability of GK-MLIP-EMD to solids. The κ_{LS} of β -Cu_{1.95}Se obtained based on GK-MLIP-EMD exhibit large deviations among different MLIP models at high temperatures, although relatively close κ_{LS} are obtained for both Mg₃Sb₂ and Mg₂Sn. The κ_{LS} obtained through the direct method show excellent repeatability among MLIP models and agree well with all available experimental results for β -Cu_{1.95}Se. The failure of the GK-MLIP-EMD approach for β -Cu_{1.95}Se is attributed to the ambiguous definition of the local atomic potential energy U_i in MLIPs, exacerbated by the diffusion of Cu atoms at elevated temperatures. This work demonstrates that high atomic diffusion is detrimental to the accuracy of GK-MLIP-EMD for thermal transport simulations, even in solids. The direct method is more suitable for predicting the κ_L in PCPL materials with severe atomic diffusion.

II. METHODS

A. Thermal transport based on MD

The methods for thermal transport simulation based on MD include the Green-Kubo method (based on EMD) and the direct method (based on NEMD). In the Green-Kubo method, the κ_L tensor along $\alpha\beta$ ($\alpha, \beta = x, y, z$) at a given correlation time t can be defined as

$$\kappa_{\alpha\beta}(t) = \frac{1}{k_B T^2 V} \int_0^\infty \langle \mathbf{J}_\alpha(0) \mathbf{J}_\beta(t) \rangle dt, \quad (1)$$

where k_B , T , and V are Boltzmann's constant, the absolute temperature, and the volume of the simulation cell, respectively. Heat flux \mathbf{J} consists of the convective term (\mathbf{J}_{conv}) and

conductive term (\mathbf{J}_{cond}), and it can be defined as

$$\mathbf{J} \equiv \frac{d}{dt} \sum_i \mathbf{r}_i E_i = \sum_i \mathbf{v}_i E_i + \sum_i \mathbf{r}_i \frac{dE_i}{dt} = \mathbf{J}_{\text{conv}} + \mathbf{J}_{\text{cond}}, \quad (2)$$

where \mathbf{r}_i , \mathbf{v}_i , and E_i are the position, velocity, and energy of atom i , respectively. The convective term and conductive term can be expressed as

$$\mathbf{J}_{\text{conv}} = \sum_i \mathbf{v}_i \left(\frac{1}{2} m_i \mathbf{v}_i^2 + U_i \right), \quad (3)$$

$$\begin{aligned} \mathbf{J}_{\text{cond}} &= \sum_i \mathbf{r}_i \frac{d}{dt} \left(\frac{1}{2} m_i \mathbf{v}_i^2 + U_i \right) \\ &= \sum_i \mathbf{r}_i (\mathbf{F}_i \cdot \mathbf{v}_i) + \sum_i \mathbf{r}_i \frac{dU_i}{dt}, \end{aligned} \quad (4)$$

where \mathbf{F}_i , m_i , and U_i are the force, mass, and local potential energy of atom i , respectively. The heat flux depends on not only the atomic force but also the potential energy of the individual atom.

In the direct method, the κ_L along the α ($\alpha = x, y, z$) axis can be defined as

$$\kappa_\alpha = \frac{\mathbf{J}}{-\frac{\partial T}{\partial \alpha}}, \quad (5)$$

where \mathbf{J} and T are the heat flux and the temperature, respectively. Different from the EMD, the heat flux in NEMD is manually applied to the system investigated. In this work, the heat flux is introduced by velocity exchanges, according to the Müller-Plathe method [17].

B. Calculation details of the GK-MLIP-EMD method

The training data sets of Mg₂Sn, Mg₃Sb₂, and Cu_{2-x}Se were obtained through the DAS [23] method. The detailed processes were presented in our previous work [23] (Mg₃Sb₂) and Supplemental Material (Mg₂Sn and Cu_{2-x}Se) [30]. Nine MLIP models of Cu_{2-x}Se with different levels and five MLIP models of Mg₂Sn and Mg₃Sb₂ were trained in the forms of the MTP. For Cu_{1.95}Se, $5 \times 5 \times 5$ (1475 atoms) supercells were selected in the MD simulations using the Green-Kubo method at 300 and 600 K. Each MD simulation was first equilibrated for 100 ps in the NPT ensemble, and then switched to the NVE ensemble for 500 ps. For Mg₂Sn and Mg₃Sb₂, $5 \times 5 \times 5$ (1500 atoms) and $8 \times 8 \times 8$ (2560 atoms) supercells were selected in the MD simulations using the Green-Kubo method. The experimental lattice constants were adopted for κ_{LS} calculations of Mg₃Sb₂ [31] and Mg₂Sn [32]. Each MD simulation was first equilibrated for 100 ps in the NVT ensemble and then switched to the NVE ensemble for 100 ps. Heat flux data were collected for 2 ns and recorded every 10 fs for all three materials. The converged correlation times of Cu_{1.95}Se, Mg₃Sb₂, and Mg₂Sn were from the periods [3, 6] ps, [50, 100] ps, and [150, 300] ps, respectively, in the MD simulations. Five independent simulations were conducted for Cu_{1.95}Se at each temperature to reduce errors, while 40 independent simulations were conducted for Mg₃Sb₂ and Mg₂Sn.

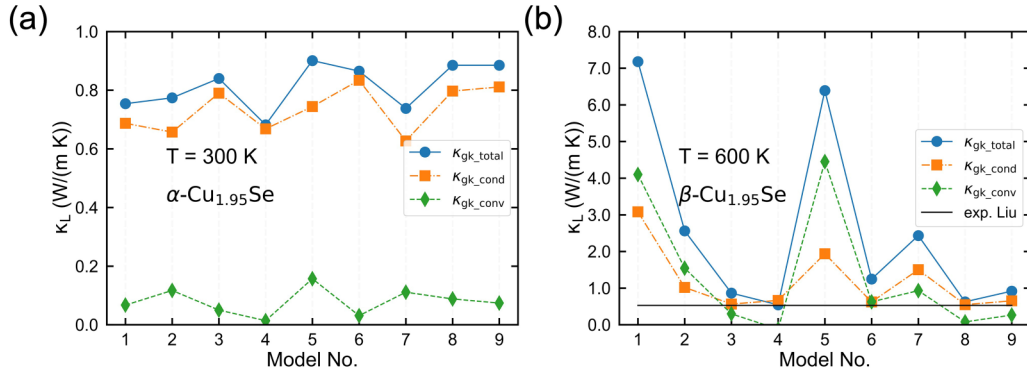


FIG. 1. GK-MLIP-EMD method for Cu_{1.95}Se. κ_L s predicted by the GK-MLIP-EMD method at (a) 300 K along the perpendicular direction and (b) 600 K with different MLIP models for Cu_{1.95}Se. The contributions of the convective term (κ_{gk_conv}) and the conductive term (κ_{gk_cond}) to κ_L are also shown. The experimental κ_L [9] is indicated by the black solid line in (b).

C. Calculation details of the direct method based on NEMD

In the direct method, the simulation size correlates with the thermal mean free path dominating phonon transport. Five sizes ($3 \times N_b \times 3$, $N_b = 24, 36, 48, 60$, and 80 for α -Cu_{1.95}Se at 300 K; $3 \times N_b \times 3$, $N_b = 20, 30, 40, 50$, and 60 for β -Cu_{1.95}Se at 600 K; $4 \times 4 \times N_c$, $N_c = 150, 160, 175, 200$, and 250 for Mg₃Sb₂ at 300 K; $4 \times 4 \times N_c$, $N_c = 100, 125, 150, 160$, and 200 for Mg₃Sb₂ at 600 K; $3 \times 3 \times N_c$, $N_c = 400, 440, 480, 540$, and 600 for Mg₂Sn at 300 K; and $3 \times 3 \times N_c$, $N_c = 360, 400, 440, 480$, and 540 for Mg₂Sn at 600 K) were used to calculate the κ_L s of all three materials. Five, two, and one independent simulations were conducted for Cu_{1.95}Se, Mg₃Sb₂, and Mg₂Sn, respectively, at each temperature to reduce errors.

III. RESULTS AND DISCUSSION

A. Lattice thermal conductivity

The crystal structures of Cu₂Se, Mg₃Sb₂, and Mg₂Sn are listed in Supplemental Material Fig. S1 [30]. The low-temperature phase structure α -Cu₂Se is still controversial (the DFT-predicted structure S3 [11,33] is shown in Supplemental Material Fig. S1(a) [30] as the initial input for sampling), and the high-temperature phase β -Cu₂Se consists of two sublattices: one is a face-centered-cubic framework constructed by Se atoms, and the other is formed by Cu atoms located at $8c$ [Supplemental Material Fig. S1(b) [30]]. Cu vacancies are randomly distributed and kept as far away from each other as possible in this case.

The MLIP models in the form of the MTP were fitted based on their effective training data sets for Mg₂Sn, Mg₃Sb₂, and Cu_{2-x}Se with the DAS method. The Supplemental Material (Figs. S2–S6 [30]) discusses the accuracy of the MLIPs for Mg₂Sn, Mg₃Sb₂, and Cu_{2-x}Se ($0 \leq x \leq 0.05$) in detail, especially in terms of the forces on the three systems and structural descriptions of Cu_{2-x}Se. The GK-MLIP-EMD approach was adopted to explore the thermal transport properties of the three materials. Figure 1 shows the total κ_L s as well as the contributions of the convective and conductive terms to κ_L s at low and high temperatures obtained with different MLIP models (e.g., MTP1 means model 1) for Cu_{1.95}Se, and the corresponding heat current autocorrelation functions are

shown in Supplemental Material Fig. S7 [30]. The average κ_L of the nine MLIP models of α -Cu_{1.95}Se is 0.82 W/mK at 300 K and the deviation among models is small (0.13 W/mK). However, the total κ_L difference among the MLIP models is up to an order of magnitude for β -Cu_{1.95}Se at 600 K, e.g., 7.18 W/mK for MTP1, and 0.54 W/mK for MTP4. The convective and conductive terms of κ_L fluctuate around their corresponding mean values for crystalline α -Cu_{1.95}Se at 300 K, but they strongly deviate for PCPL β -Cu_{1.95}Se at 600 K, which is rare in crystalline solids. Moreover, although there is an order of magnitude difference in κ_L between MTP1 and MTP3 for β -Cu_{1.95}Se, the convective terms grow with temperature in both models (Supplemental Material Fig. S8 [30]). These results demonstrate a non-negligible contribution of the convective term to the κ_L in β -Cu_{1.95}Se. In addition, defects have little effect on κ_L and are not the cause of the κ_L deviation among the MLIP models (Supplemental Material Fig. S9 [30]).

The average κ_L s of the comparison material Mg₂Sn (Supplemental Material Fig. S10 [30]) are 7.10 W/mK at 300 K and 2.83 W/mK at 600 K, which are consistent with the experimental values reported in the reference (7.19 and 3.43 W/mK at 300 and 600 K [34]). The contribution of the convective term is always below 4%, even at high temperatures, due to the small displacement near the equilibrium position in Mg₂Sn. For Mg₃Sb₂, which contains asymmetrical displacement of tetragonal Mg atoms at high temperatures, the average κ_L decreases from 1.88 W/mK at 300 K to 1.01 W/mK at 600 K. The average contribution of convective terms increases from 4% at 300 K to 9% at 600 K, and the deviation among models is within 0.18 W/mK. The low contributions of the convective terms in the two crystalline compounds are in contrast to the case of β -Cu_{1.95}Se shown above. The theoretical κ_L s of Mg₃Sb₂ are consistent with the experimental values, which are 1.62 and 1.12 W/mK at 300 and 600 K, respectively [35].

In contrast, as shown in Fig. 2(a), the κ_L of β -Cu_{1.95}Se can be accurately described by the direct method based on NEMD. Unlike the GK-MLIP-EMD method, the κ_L s obtained with different MLIP models through the direct method are almost identical under the same size, even for the high-temperature β -phase (Supplemental Material Fig. S11 [30]): for example, $\kappa_{direct} = 0.47$ W/mK with a length of 11.54 nm at 600 K, and the deviation for β -Cu_{1.95}Se among the nine MLIP models

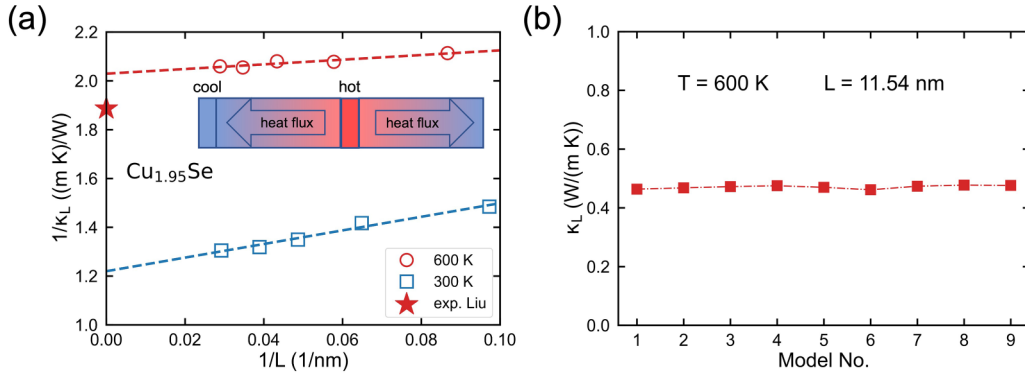


FIG. 2. Direct method based on the MLIP for $\text{Cu}_{1.95}\text{Se}$. (a) Length-dependent κ_{LS} for $\text{Cu}_{1.95}\text{Se}$ at different temperatures compared with the available experimental value [9] of $\beta\text{-Cu}_{1.95}\text{Se}$ at 600 K. The illustration shows a schematic diagram of the direct method. (b) The κ_{LS} predicted by the direct method with different MLIP models at 600 K ($3 \times 3 \times 20$ supercells) in $\text{Cu}_{1.95}\text{Se}$.

is within 0.01 W/mK [Fig. 2(b)]. This is distinct from the GK-MLIP-EMD behavior, as mentioned above. The existence of vacancies will reduce κ_L by 11% on average but will not increase the small deviation among different MLIP models. The κ_L obtained through the direct method at 300 K extrapolated to infinity is 0.83 ± 0.02 W/mK, close to the value of 0.82 ± 0.06 W/mK obtained through the GK-MLIP-EMD method for $\alpha\text{-Cu}_{1.95}\text{Se}$. The κ_L obtained through the direct method at 600 K is 0.49 ± 0.01 W/mK, which agrees well with the available experimental results [9]. The κ_{LS} of Mg_2Sn and Mg_3Sb_2 calculated by the direct method are 6.65 and 3.72 W/mK and 1.69 and 0.97 W/mK at 300 and 600 K (Supplemental Material Fig. S12 [30]). The direct method is generally applicable to all types of materials.

B. Ambiguous projection of local atomic potential energy U_i

The reason why the GK-MLIP-EMD approach fails for the high-temperature phase $\beta\text{-Cu}_{1.95}\text{Se}$ deserves further rationalization. Generally, the deviation of κ_L obtained based on the GK-MLIP-EMD method could originate from several key quantities, including the atomic velocity or position, or U_i , or the training process itself, i.e., the loss function. We used controlled comparisons to clarify the influence of the key quantities causing the failure of the GK-MLIP-EMD approach in the evaluation of κ_{LS} for PCPL $\beta\text{-Cu}_{1.95}\text{Se}$.

We performed MD simulations with MTP3 of $\text{Cu}_{1.95}\text{Se}$ and fixed the velocities and positions of atoms, and then calculated the κ_{LS} with other MLIP models, as shown in Figs. 3(a) and 3(b). In this process, the fixed velocities and positions are all from MTP3, but U_i is generated by the respective MLIP models. After fixing the velocities and positions, the deviation of κ_{LS} among MLIP models is still small, within the value of 0.09 W/mK for $\alpha\text{-Cu}_{1.95}\text{Se}$ at 300 K. The results are similar to those without the fixed velocities and positions. For PCPL $\beta\text{-Cu}_{1.95}\text{Se}$, close κ_{LS} are obtained when the same MLIP model (resulting in similar U_i) with different velocities and positions, for example, $\kappa_{\text{gk}} = 7.18$ W/mK and $\kappa_{\text{gk,fix}} = 6.95$ W/mK in MTP1. However, diverse κ_{LS} are obtained when different MLIP models (resulting in different U_i) along with the same velocities and positions, for example, $\kappa_{\text{gk,fix}} = 6.95$ W/mK in MTP1 and $\kappa_{\text{gk,fix}} = 0.89$ W/mK in MTP3. The clear comparison indicates that the deviation of

the κ_{LS} of $\beta\text{-Cu}_{1.95}\text{Se}$ among different MLIP models cannot be attributed to the velocity and position; U_i is responsible for the deviations, as seen below.

Supplemental Material Fig. S13 [30] extracts the U_i of a transient structure from MD simulations and demonstrates that U_i exhibits arbitrariness (U_i varies among MLIP models for the same atom) in $\text{Cu}_{1.95}\text{Se}$ at both low and high temperatures. The corresponding U_i distributions are shown in Figs. 3(c) and 3(d). In MTP1 and MTP2, the U_i of Cu atoms is relatively low, while the U_i of Se atoms is close to the high-energy end. However, the order is reversed in MTP3. In contrast, the U_i distributions predicted by the same MLIP model at different temperatures have great similarity. For example, the relative positions of peaks are nearly fixed at 300 K compared with those at 600 K, only with different smearing. More importantly, the arbitrariness of U_i also occurs in Mg_2Sn and Mg_3Sb_2 (Supplemental Material Fig. S14 [30]). For the same model, the peak position of U_i is not changed but the width is broadened with increasing temperature. In other words, the arbitrariness of U_i is common in MLIPs, but its influence on κ_L through the GK-MLIP-EMD approach depends on the material.

Another possible cause is the loss function, representing how well the MLIP model fits, which involves the total energy, atomic forces, and stress tensor. The loss functions of the three materials with different MLIP models converge to close values after several hundred training cycles (Supplemental Material Fig. S15 [30]). Although there is an ambiguous projection of U_i , the total potential energy can always be preserved by adopting adjustment of parameters. The ambiguous projection of U_i does not affect the loss function as long as the total potential energy remains unchanged according to $E_i = \frac{1}{2}m_i\mathbf{v}_i^2 + U_i$. For $\text{Cu}_{1.95}\text{Se}$, the mean absolute errors of the total potential energy [Supplemental Material Fig. S16(a) [30]] between the other models and MTP3 are approximately 0.6 and 1.0 meV/atom at 300 and 600 K, respectively. The mean absolute errors of the atomic forces [Supplemental Material Fig. S16(b) [30]] predicted by the other models and MTP3 are approximately 30 and 54 meV/Å at 300 and 600 K, respectively. Therefore, all MLIP models are accurate in terms of total potential energy and atomic forces, and the deviation of κ_{LS} among the MLIP models is not related to the training process itself. Similar small mean absolute errors

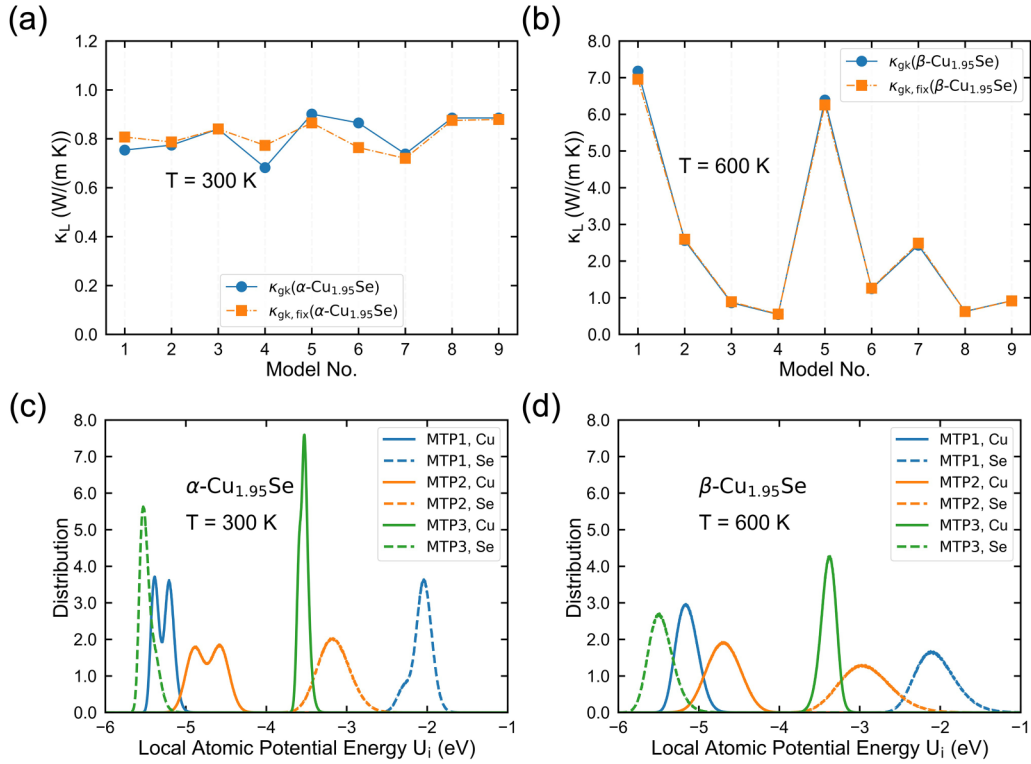


FIG. 3. Ambiguous projection of U_i , $\kappa_L S$ of $\text{Cu}_{1.95}\text{Se}$ predicted by the GK-MLIP-EMD approach with/without fixed positions and velocities (generated from the MD simulations with MTP3) at (a) 300 K and (b) 600 K in $\text{Cu}_{1.95}\text{Se}$. $\kappa_{\text{gk,fix}}$ means κ_L predicted with fixed positions and velocities but using their own U_i . κ_{gk} means κ_L predicted without fixed positions and velocities using their own U_i . U_i distributions of Cu and Se atoms are achieved from MD simulations at (c) 300 K and (d) 600 K in $\text{Cu}_{1.95}\text{Se}$. MTP1, MTP2, and MTP3 are the first three MLIP models.

of the total potential energy and atomic forces are also found for Mg_2Sn and Mg_3Sb_2 , as shown in Supplemental Material Fig. S17 [30].

C. Atomic diffusion

Why the applicability of the GK-MLIP-EMD method depends on the material relates to the atomic movements in solids. In principle, the magnitude of the atom deviation from the equilibrium position is commonly estimated by the mean square displacement (MSD). Figure 4(a) shows the

relationship between the MSD (obtained from second-order force constants in crystalline materials) and the average atomic mass for thermoelectric materials and some other typical semiconductors (some from the literature [36]). Typical semiconductors are mainly harmonic materials with a small MSD, while thermoelectric materials possess a relatively large MSD, which leads to a low κ_L . The MSD values of PCPL materials are infinitely large due to the atomic diffusion. The corresponding atomic trajectories of Mg_2Sn , Mg_3Sb_2 , and $\beta\text{-Cu}_{1.95}\text{Se}$ can visualize how atoms vibrate at finite temperatures, as shown in Fig. 4(b). The atomic displacements

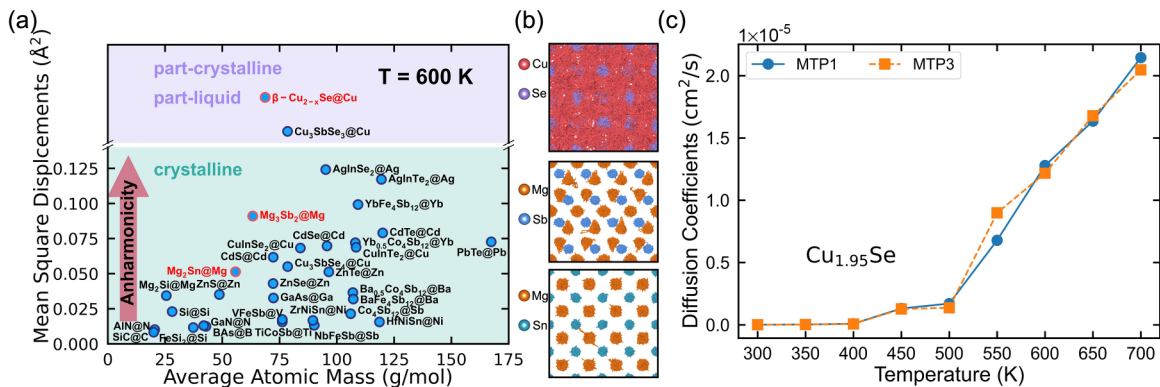


FIG. 4. Atomic diffusion for different types of solids. (a) Relationship between MSDs and the average atomic mass for thermoelectric materials and some other typical semiconductor compounds; (b) atomic trajectories of Mg_2Sn , Mg_3Sb_2 , and $\beta\text{-Cu}_{1.95}\text{Se}$ at high temperatures; (c) diffusion coefficient of Cu atoms at different temperatures obtained with MTP1 and MTP3.

are located nearly at the equilibrium position for Mg_2Sn , while the displacement of tetrahedral Mg atoms becomes anisotropic for Mg_3Sb_2 at high temperatures [35]. Moreover, Cu atoms jump back and forth between interstitial positions while Se atoms are located at the equilibrium position for $\beta\text{-Cu}_{1.95}\text{Se}$, demonstrating the PCPL state and exhibiting the strongest chemical bond hierarchy among these materials. The unique trajectory relates to the atomic diffusion in $\beta\text{-Cu}_{1.95}\text{Se}$, as shown below.

The temperature-dependent diffusion coefficient of Cu atoms is shown in Fig. 4(c). The diffusion coefficient of Cu atoms is approximately $10^{-8} \text{ cm}^2/\text{s}$ in the α phase, and then rises to approximately $10^{-6} \text{ cm}^2/\text{s}$ in the phase transition range 450-550 K. Above 550 K, the diffusion coefficient of Cu atoms reaches $10^{-5} \text{ cm}^2/\text{s}$ in the high-temperature β phase. Such a tremendous diffusion coefficient of Cu atoms is in sharp contrast to that of Se atoms with a value less than $10^{-8} \text{ cm}^2/\text{s}$ in the temperature range 300-700 K, as shown in Supplemental Material Fig. S18 [30], which also confirms the PCPL state in $\beta\text{-Cu}_{1.95}\text{Se}$. The diffusion coefficients in Mg_2Sn are $10^{-11} \text{ cm}^2/\text{s}$ for both Mg and Sn atoms. The diffusion coefficient of Mg atoms with asymmetric displacement at high temperatures in Mg_3Sb_2 is approximately $10^{-8} \text{ cm}^2/\text{s}$, which is larger than that in Mg_2Sn , whereas the diffusion coefficient of Sb atoms is approximately $10^{-10} \text{ cm}^2/\text{s}$ due to the relatively heavy mass.

Ranninger *et al.* [37] proposed that the contribution of the convective term becomes non-negligible when the displacement of the atom from the equilibrium position is comparable to the nearest interatomic spacing. The small diffusion coefficient of atoms, such as for Mg_2Sn and Mg_3Sb_2 , thus causes a small contribution of the convective term to κ_L in the GK-MLIP-EMD method. However, the diffusion coefficient of Cu atoms in $\beta\text{-Cu}_{1.95}\text{Se}$ is so large that the contribution of the convective term cannot be neglected. As the diffusion coefficient increases, the contribution of the convective term increases (Supplemental Material Fig. S8 [30]). In addition, a small diffusion coefficient leads to a tiny contribution of $\mathbf{r}_i \frac{dU_i}{dt}$ in the conductive term [Eq. (4)]. However, for $\beta\text{-Cu}_{1.95}\text{Se}$ the contribution of $\mathbf{r}_i \frac{dU_i}{dt}$ becomes strongly fluctuating among different MLIP models due to the large displacements (or large \mathbf{r}_i) of Cu atoms (Supplemental Material Fig. S19 [30]). According to Eqs. (3) and (4), the accuracy of the convective term and conductive term in the Green-Kubo equation is largely determined by U_i ; thus, the ambiguous projection of U_i will break down the GK-MLIP-EMD approach due to its influence on both the convective and conductive terms.

In summary, the ambiguous projection of U_i in MLIPs, exacerbated by atomic diffusion, is the fundamental reason for the failure of GK-MLIP-EMD in predicting the κ_L for PCPL $\beta\text{-Cu}_{1.95}\text{Se}$. The ambiguous definition of U_i is an inherent problem in MLIPs. This leads to the arbitrariness of the convective term and the conductive term within the GK-MLIP-EMD method; but for most solid materials, the in-

fluence is negligible. The uncertainty in the thermal transport prediction for the GK-MLIP-EMD method is closely related to the atomic displacements. The calculated κ_L is hardly affected for Mg_2Sn and slightly influenced for Mg_3Sb_2 at high temperatures. However, when the atomic displacements reach a certain level at finite temperatures, the GK-MLIP-EMD approach completely breaks down, such as for $\beta\text{-Cu}_{1.95}\text{Se}$ with Cu diffusion at high temperatures. This phenomenon can be extended to other similar solid materials with severe atomic diffusion, such as argyrodite-type thermoelectrics [38] and lithium-ion battery materials [39].

IV. CONCLUSIONS

The κ_L s of PCPL $\beta\text{-Cu}_{1.95}\text{Se}$ obtained through the GK-MLIP-EMD method based on different MLIP models highly deviate, and thus are not reliable at high temperatures. In contrast, when the direct method is adopted to calculate κ_L , the results are consistent with available experimental values. The GK-MLIP-EMD approach fails for $\beta\text{-Cu}_{1.95}\text{Se}$ due to the ambiguous definition of U_i in MLIPs, worsened by the existence of Cu diffusion. The ambiguous projection of U_i is common in MLIPs, and it greatly affects the convective and the conductive terms of the Green-Kubo theory. Because of the large contribution of the convective term to κ_L and the fluctuating conductive term arising from Cu diffusion in $\beta\text{-Cu}_{1.95}\text{Se}$, GK-MLIP-EMD thus fails to describe the thermal transport of this compound. The present work elucidates the fact that the ambiguous projection of U_i leads to failure of thermal transport application of the GK-MLIP-EMD method to solids with severe atomic diffusion.

ACKNOWLEDGMENTS

This work was supported by the National Natural Science Foundation of China (Grants No. 52172216 and No. 92163212) and the Key Research Project of Zhejiang Laboratory (No. 2021PE0AC02). W.Q.Z. also acknowledges the support from the Guangdong Innovation Research Team Project (Grant No. 2017ZT07C062), Shenzhen Municipal Key-Lab program (Grant No. ZDSYS20190902092905285), Guangdong Provincial Key-Lab program (Grant No. 2019B030301001), Guangdong Major Talent Project Introduction Category (Grant No. 2019CX01C237), and Centers for Mechanical Engineering Research and Education at MIT and SUSTech. Part of the computing resources are supported by the Center for Computational Science and Engineering at SUSTech.

Y.Z., E.D., H.Y., J.Y., and W.Z. designed the research; Y.Z., E.D., H.Y., J.Y., and W.Z. performed the research; Y.Z., E.D., H.Y., L.X., J.Y., and W.Z. analyzed the data; and Y.Z., J.Y., and W.Z. wrote the paper. The authors declare no competing interest.

[1] X. Qian, J. Zhou, and G. Chen, Phonon-engineered extreme thermal conductivity materials, *Nat. Mater.* **20**, 1188 (2021).

[2] T. M. Tritt, *Thermal Conductivity: Theory, Properties, and Applications* (Kluwer Academic/Plenum, New York, 2004).

- [3] W. Li, J. Carrete, A. Katcho, N. Sheng *et al.*, BTE: A solver of the Boltzmann transport equation for phonons, *Comput. Phys. Commun.* **185**, 1747 (2014).
- [4] A. Togo, L. Chaput, and I. Tanaka, Distributions of phonon lifetimes in Brillouin zones, *Phys. Rev. B* **91**, 094306 (2015).
- [5] Y. Xia, V. I. Hegde, K. Pal, X. Hua, D. Gaines, S. Patel, J. He, M. Aykol, and C. Wolverton, High-Throughput Study of Lattice Thermal Conductivity in Binary Rocksalt and Zinc Blende Compounds Including Higher-Order Anharmonicity, *Phys. Rev. X* **10**, 041029 (2020).
- [6] Y. Xia, K. Pal, J. He, V. Ozoliņš, and C. Wolverton, Particlelike Phonon Propagation Dominates Ultralow Lattice Thermal Conductivity in Crystalline Ti_3VSe_4 , *Phys. Rev. Lett.* **124**, 065901 (2020).
- [7] W. Qiu, L. Xi, P. Wei *et al.*, Part-crystalline part-liquid state and rattling-like thermal damping in materials with chemical-bond hierarchy, *Proc. Nat. Acad. Sci. USA* **111**, 15031 (2014).
- [8] H. Kim, S. Ballikaya, H. Chi *et al.*, Ultralow thermal conductivity of $\beta\text{-Cu}_2\text{Se}$ by atomic fluidity and structure distortion, *Acta Mater.* **86**, 247 (2015).
- [9] H. Liu, X. Shi, F. Xu *et al.*, Copper ion liquid-like thermoelectrics, *Nat. Mater.* **11**, 422 (2012).
- [10] P. Qiu, T. Mao, Z. Huang *et al.*, High-efficiency and stable thermoelectric module based on liquid-like materials, *Joule* **3**, 1538 (2019).
- [11] W. Qiu, P. Lu, X. Yuan *et al.*, Structure family and polymorphous phase transition in the compounds with soft sublattice: Cu_2Se as an example, *J. Chem. Phys.* **144**, 194502 (2016).
- [12] M. P. Allen and D. J. Tildesley, *Computer Simulation of Liquids* (Oxford University Press, Oxford, 2017).
- [13] M. S. Green, Markoff random processes and the statistical mechanics of time-dependent phenomena. II. Irreversible processes in fluids, *J. Chem. Phys.* **22**, 398 (1954).
- [14] R. Kubo, Statistical-mechanical theory of irreversible processes. I. General theory and simple application to magnetic and conduction problems, *J. Phys. Soc. Jpn.* **12**, 570 (1957).
- [15] S. Nosé, A unified formulation of the constant temperature molecular dynamics methods, *J. Chem. Phys.* **81**, 511 (1984).
- [16] T. Ikeshoji and B. Hafskjold, Non-equilibrium molecular dynamics calculation of heat conduction in liquid and through liquid-gas interface, *Mol. Phys.* **81**, 251 (1994).
- [17] F. Müller-Plathe, A simple nonequilibrium molecular dynamics method for calculating the thermal conductivity, *J. Chem. Phys.* **106**, 6082 (1997).
- [18] J. Behler, Constructing high-dimensional neural network potentials: A tutorial review, *Int. J. Quantum Chem.* **115**, 1032 (2015).
- [19] A. P. Bartók and G. Csányi, Gaussian approximation potentials: A brief tutorial introduction, *Int. J. Quantum Chem.* **115**, 1051 (2015).
- [20] H. Wang, L. Zhang, J. Han *et al.*, DeePMD-kit: A deep learning package for many-body potential energy representation and molecular dynamics, *Comput. Phys. Commun.* **228**, 178 (2018).
- [21] A. V. Shapeev, Moment tensor potentials: A class of systematically improvable interatomic potentials, *Multiscale Model. Simul.* **14**, 1153 (2016).
- [22] L. Zhang, D.-Y. Lin, H. Wang, R. Car, and W. E, Active learning of uniformly accurate interatomic potentials for materials simulation, *Phys. Rev. Mater.* **3**, 023804 (2019).
- [23] H. Yang, Y. Zhu, E. Dong, Y. Wu, J. Yang, and W. Zhang, Dual adaptive sampling and machine learning interatomic potentials for modeling materials with chemical bond hierarchy, *Phys. Rev. B* **104**, 094310 (2021).
- [24] C. W. Rosenbrock, K. Gubaev, A. V. Shapeev *et al.*, Machine-learned interatomic potentials for alloys and alloy phase diagrams, *npj Comput. Mater.* **7**, 24 (2021).
- [25] S. Ma, S.-D. Huang, and Z.-P. Liu, Dynamic coordination of cations and catalytic selectivity on zinc-chromium oxide alloys during syngas conversion, *Nat. Catal.* **2**, 671 (2019).
- [26] M. Li, G. Cao, Y. Luo *et al.*, Predicting the lattice thermal conductivity of alloyed compounds from the perspective of configurational entropy, *npj Comput. Mater.* **8**, 75 (2022).
- [27] P. Korotaev, I. Novoselov, A. Yamilkin, and A. Shapeev, Accessing thermal conductivity of complex compounds by machine learning interatomic potentials, *Phys. Rev. B* **100**, 144308 (2019).
- [28] R. Bertossa, F. Grasselli, L. Ercole, and S. Baroni, Theory and Numerical Simulation of Heat Transport in Multicomponent Systems, *Phys. Rev. Lett.* **122**, 255901 (2019).
- [29] B. Cheng and D. Frenkel, Computing the Heat Conductivity of Fluids from Density Fluctuations, *Phys. Rev. Lett.* **125**, 130602 (2020).
- [30] See Supplemental Material at <http://link.aps.org/supplemental/10.1103/PhysRevB.108.014108> for the parameter settings of the sampling processes; the accuracy of machine-learning interatomic potentials; the effect of vacancies on lattice thermal conductivity for $\text{Cu}_{1.95}\text{Se}$; the local atomic potential energies; and the lattice thermal conductivities for comparison systems Mg_2Sn and Mg_3Sb_2 .
- [31] J. Zhang, L. Song, M. Sist *et al.*, Chemical bonding origin of the unexpected isotropic physical properties in thermoelectric Mg_3Sb_2 and related materials, *Nat. Commun.* **9**, 4716 (2018).
- [32] H. Kasai, L. Song, H. L. Andersen *et al.*, Multi-temperature structure of thermoelectric Mg_2Si and Mg_2Sn , *Acta Crystallogr. Sect. B: Struct. Sci.* **73**, 1158 (2017).
- [33] P. Lu, H. Liu, X. Yuan *et al.*, Multiformity and fluctuation of Cu ordering in Cu_2Se thermoelectric materials, *J. Mater. Chem. A* **3**, 6901 (2015).
- [34] J. J. Martin, Thermal conductivity of Mg_2Si , Mg_2Ge and Mg_2Sn , *J. Phys. Chem. Solids* **33**, 1139 (1972).
- [35] Y. Zhu, Y. Xia, Y. Wang *et al.*, Violation of the T^{-1} relationship in the lattice thermal conductivity of Mg_3Sb_2 with locally asymmetric vibrations, *Research* **2020**, 4589786 (2020).
- [36] A. Togo and I. Tanaka, First principles phonon calculations in materials science, *Scr. Mater.* **108**, 1 (2015).
- [37] J. Ranninger, Lattice thermal conductivity, *Phys. Rev.* **140**, A2031 (1965).
- [38] X. Qi, J. Chen, K. Guo *et al.*, Thermal stability of Ag_9GaSe_6 and its potential as a functionally graded thermoelectric material, *Chem. Eng. J.* **374**, 494 (2019).
- [39] X. He, Y. Zhu, A. Epstein *et al.*, Statistical variances of diffusional properties from ab initio molecular dynamics simulations, *npj Comput. Mater.* **4**, 18 (2018).